ELSEVIER

Journal of Nuclear Materials 290–293 (2001) 281–285

journal of nuclear materials

www.elsevier.nl/locate/jnucmat

Rapid diffusion of lithium into bulk graphite in lithium conditioning

N. Itou [a], H. Toyoda [a], K. Morita [b], H. Sugai [a,*]

[a] *Department of Electrical Engineering, Furo-cho, Chikusa-ku, Nagoya 464-8603, Japan*
[b] *Department of Crystalline Materials Science, Furo-cho, Chikusa-ku, Nagoya 464-8603, Japan*

Abstract

One of the known lithium conditioning effects is the reduction of carbon impurities released from the graphite walls of a tokamak. However, little is known about the role of lithium in graphite–plasma interactions. Graphite intercalates lithium atoms between the hexagonal layer planes. The Li diffusion constant in the direction perpendicular to the basal planes of highly oriented pyrolytic graphite (HOPG) is measured for the first time using Rutherford backscattering spectrometry and is found to be $D_{\perp} = 2.1 \times 10^{-10}$ cm^2/s with an activation energy of 0.26 eV, in the case of low temperatures (300 K) and low Li concentration (Li/C atomic ratio <3%). This value increases by a factor of two when HOPG is exposed to hydrogen plasma before lithium deposition. The implications resulting from the Li–graphite intercalation in lithium wall conditioning are discussed, focusing on Li-induced suppression of graphite sputtering.

Keywords: Lithium coating; Carbon; Lithium

1. Introduction

The observed effects of wall conditioning by in-situ lithium deposition are very low hydrogen recycling, reduction of oxygen impurity in a hot core plasma region, significant suppression of carbon impurity, and improvement of energy confinement. Although these effects have been markedly observed in TFTR [1,2], this is not the case in other machines [3–5]. These differences must be reconciled and the underlying physics and chemistry of lithium effects must be clarified.

Efforts to elucidate the roles of lithium in wall conditioning have been made in the previous studies [3,5,6]. A strong chemical activity of a fresh lithium layer was observed, which could successfully account for the hydrogen pumping effect by lithium hydride (LiH) formation and for the oxygen gettering effect by lithium oxide (Li_2O) formation. As far as carbon impurity released from graphite walls is concerned, previous studies [5] revealed that the lithium conditioning suppresses the physical sputtering yield of graphite by an order of magnitude, forming *graphite intercalation compounds* (GICs) with deep penetration of lithium in graphite as observed in DIII-D [7] and TFTR [8].

Graphite is known to intercalate lithium up to a maximum of 1 lithium atom per six carbon atoms, and to form LiC_6, which is called the stage-one Li–GIC. This property has been used in lithium-ion batteries whose negative electrodes are made of graphite. The anisotropic diffusion constants of lithium atom in graphite have been investigated [9–16]. However, most of the previous studies are limited to a regime of high temperatures (~700 K) and high concentration ($x = 1$ in Li_xC_6).

In this paper, we report the results of a study that was done to determine the perpendicular diffusion constant of lithium in graphite at low temperatures (300 K) and low concentrations ($x \ll 1$), together with the influence of the hydrogen retention on the diffusion constant.

* Corresponding author. Tel.: +81-52 789 4697; fax: +81-52 789 3150.
E-mail address: sugai@nuee.nagoya-u.ac.jp (H. Sugai).

0022-3115/01/$ - see front matter
PII: S0022-3115(00)00630-9

2. Diffusion of lithium in graphite

2.1. Experimental

Intercalation processes of lithium atoms into graphite at room temperature are investigated in a vacuum vessel which is combined with a high-energy ion beam system for Rutherford backscattering spectrometry (RBS) measurements [15]. Highly oriented pyrolytic graphite (HOPG) [17] was selected owing to its simple structure, for measuring the Li diffusion constant $D_\perp$ in the direction perpendicular to the basal plane. Vacuum evaporation of metallic lithium (94.1% ^{7}Li + 5.9% ^{6}Li) at ~800 K and 1×10^{-6} Torr gives deposition of ~3-μm thick Li layer onto the HOPG specimen of $0.26 \times 20 \times 20$ mm^3 mounted on a rotatable stage. Special care was given to prevent the parallel diffusion ($D_\parallel$) of lithium atoms from the edge of HOPG, by masking the edge prior to the lithium deposition. The speciemen was exposed to 1 MeV proton beam at 45° incidence to obtain better spatial resolution, and the backscattered H^+ ions are detected at an angle of 10° with respect to the beam axis. After the lithium deposition is completed, the RBS measurements immediately start to get the time variation of Li atom density profile. In order to examine the influence of hydrogen retention on the Li diffusion in graphite, a hydrogen-free as-received HOPG specimen is compared with hydrogen-containing HOPG specimen which is prepared by 60-min exposure to hydrogen glow discharge plasma (300 V, 40 μA/cm^2, 20 m Torr) in the vessel. The hydrogen retention is estimated to be 8×10^{16} H/cm^2, assuming that 9% of ion fluence is retained in the graphite [16].

2.2. Lithium diffusion in hydrogen-free HOPG

Typical energy spectra of H^+ ions backscattered from a hydrogen-free HOPG at different times after lithium deposition are shown in Fig. 1. Here, the time $t = 0$ refers to the initiation of two-min lithium deposition phase. The dashed lines in Fig. 1 indicate the reference data of pure HOPG (no lithium deposition), showing a characteristic knee at the energy $E = 0.72$ MeV (scattering from the top surface carbon for 1 MeV proton incidence). In the top spectrum at $t = 4$ min, one can see that thick Li layer deposition modifies the energy spectra in two ways. The first is the down-shift ($\Delta E \sim 0.05$ MeV) of the carbon-induced spectra, owing to the energy loss in the Li layer. The second is the appearance of a new hump in a range of energy, $0.45 < E < 0.56$ MeV, corresponding to the H^+ scattering by lithium atoms. As the time goes on, the Li-induced hump gradually shrinks and becomes almost stationary after 30 min. This stationary hump suggests the formation of a lithium oxide, e.g., by reaction with the background water vapor. In fact, a small signal grows after >20 min just below the

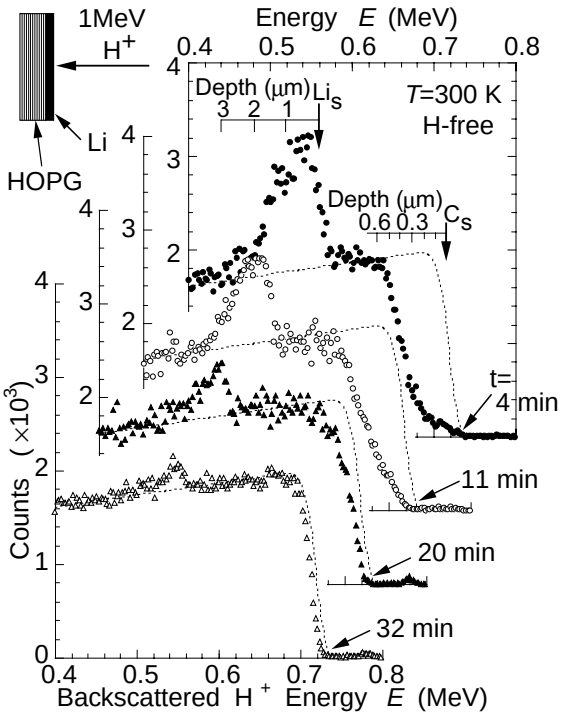

Fig. 1. RBS energy spectra for different times after lithium deposition onto the hydrogen-free HOPG at room temperature. The upper insertions indicate the scale of depth from surface carbon C_S and surface lithium Li_S.

predicted energy $E = 0.78$ MeV due to scattering by oxygen atoms. The cross-section for 1 MeV proton collision with oxygen was compared with that for proton–lithium collision, taking account of nuclear reactions of ^{7}Li and ^{6}Li. These cross-section data roughly explain the signal intensity ratio between the oxygen-induced hump and the Li-induced hump in steady-state.

The distribution of lithium concentration $c(x,t)$ can be derived from the RBS data shown in Fig. 1, where the position x is the depth from the HOPG surface. For this, first, the energy scale in Fig. 1 needs to be replaced by the depth scale as shown in the top left inset in Fig. 1; second, by subtracting the counts given by the dashed line from the measured total counts one obtains the counts $h(x,t)$ for the lithium-induced hump. This signal $h(x,t)$ is approximately proportional to $c(x,t)$, since change in the stopping power dE/dx is negligible in a narrow energy range ($\Delta E < 0.1$ MeV). Finally, the value of $h(x,t)$ is converted to the absolute Li density $c(x,t)$ as follows. Lithium vapor condenses on the HOPG surface and forms a thin layer of metallic lithium (specific gravity 0.534, atomic density $c_0 = 4.63 \times 10^{22}$ cm^{-3}). At $t = 4$ min, most of the deposited lithium still remain in a state of metallic lithium, and comparison of the peak value of h with c_0 leads to the calibration factor.

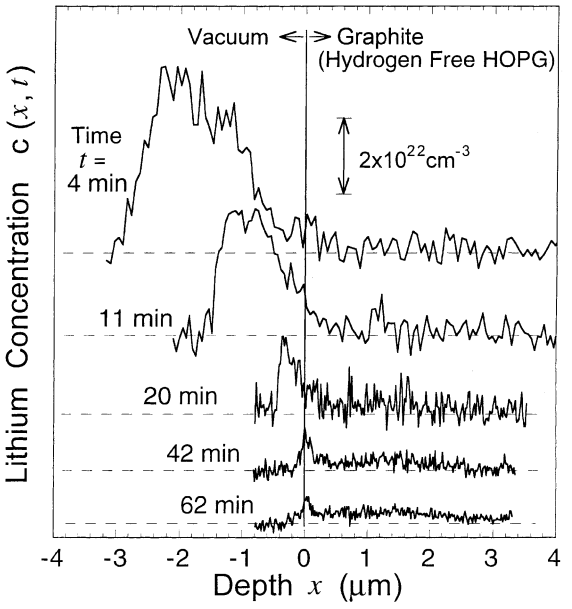

Fig. 2. Lithium concentration $c(x,t)$ as a function of depth x from the HOPG surface at different times t.

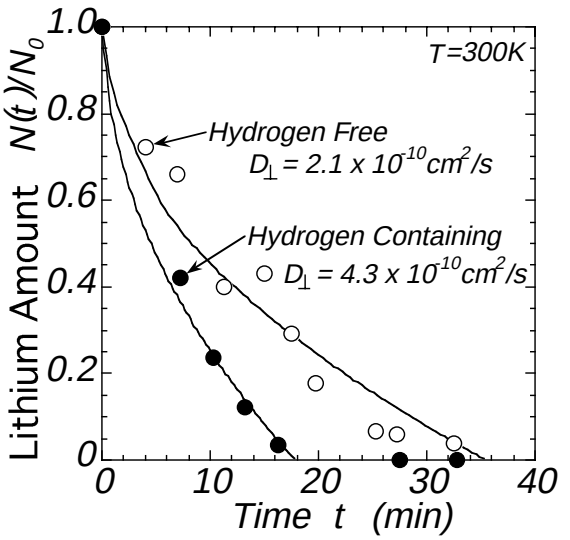

Fig. 3. Experimental points and theoretical curves for total number $N(t)$ of lithium atoms outside the HOPG as a function of time t.

The Li concentration $c(x,t)$ obtained in this way is shown in Fig. 2. Here, the location of the HOPG surface ($x = 0$) was determined as follows. The lithium–graphite intercalation theory predicts that a maximum Li concentration c_M is given by LiC_6 and hence $c_M = 1.83 \times 10^{22}$ cm^{-3} from the specific gravity 2.19 of the present HOPG. Thus, we assign the boundary $x = 0$ at the position having $c \sim c_M$. In Fig. 2, the lithium on the external surface of the HOPG specimen ($x < 0$) disappears after ~30 min, leaving lithium oxide compounds on the HOPG surface with a low concentration of lithium (~3% of carbon concentration) inside the HOPG. Previous Auger depth profiles [5] showed very large values (40% at maximum) of Li/C atomic ratio inside the graphite, however this difference can be probably caused by the radiation-induced sputtering of lithium in the sputter Auger measurements. The total number $N(t)$ of lithium atoms outside the graphite surface ($x < 0$) is calculated from $N(t) = \int_{-\infty}^{0} c(x,t)\,dx$, substituting the measured $c(x,t)$ in Fig. 2. The values of $N(t)$ normalized with the initial value N_0 are plotted in Fig. 3.

2.3. Calculation of lithium diffusion loss

The temporal decrease of $N(t)$ would be easily calculated if the Li diffusion flux through the interface ($x = 0$) from a lithium layer to the HOPG could be calculated from the diffusion equation $\partial c/\partial t = D_\perp \partial^2 c/\partial x^2$ for the lithium concentration $c(x,t)$. To solve this one-dimensional equation, we assume the following initial conditions at $t = 0$: $c = c_0$ for $x < 0$, and $c = 0$ for $x > 0$. Thus, we assume an initially empty HOPG layer contacting at $x = 0$ with a semi-infinite lithium layer of atomic density c_0. In addition, as boundary conditions we assume $c = c_M$ at $x = 0$, and $\partial c/\partial x = 0$ at $x = d$. Namely, the Li concentration at the interface $x = 0$ is equal to the maximum value c_M, and Li atoms cannot leave the opposite end of the HOPG layer.

Under these conditions, the diffusion equation can be solved and yield the following solution [18]:

$$c(x,t) = c_M - \frac{4c_M}{\pi}\sum_{m=0}^{\infty}\frac{1}{2m+1}\sin\frac{2m+1}{2d}\pi x \times \exp\left[-D_\perp\left(\frac{2m+1}{2d}\pi\right)^2 t\right]. \quad (1)$$

Numerical calculations of Eq. (1) demonstrate that Li atoms gradually diffuse into the HOPG with the diffusion time of $\sim(2d/\pi)^2/D_\perp$. In steady state ($t \to \infty$), the second term on the right-hand side vanishes and hence $c = c_M$, i.e., the HOPG is uniformly filled with lithium up to the maximum level of c_M, thus forming the stage-one intercalation compound LiC_6.

If the effect of surface barriers, such as lithium oxide, is negligible, then the lithium flux diffusing into the HOPG is given by $\Gamma(t) = -D_\perp \partial c/\partial x|_{x=0}$. If one let the areal density of deposited lithium at $t = 0$ be N_0, then, the lithium diffusion into the HOPG depletes the lithium areal density $N(t)$ outside the HOPG, which can be expressed as follows: $N(t) = N_0 - \int_0^t \Gamma(\tau)\,d\tau$. Using the solution (1), we can calculate $N(t)/N_0$ for the experimental conditions of interest (see the solid lines in Fig. 3).

The model results predict values of $N(t) < 0$ since the deposited lithium (~3-μm thick) in the present experiment is only 3% of the Li amount necessary for forming LiC_6 of thickness $d = 2600$ μm. The value of $D_\perp$ that best fits the experimental points for the hydrogen free HOPG was found to be $D_\perp = 2.1 \times 10^{-10}$ cm^2/s. The diffusion time scale τ_L, i.e., characteristic time of lithium loss is given by $\tau_L = (2l/\pi)^2/D_\perp$, where l is the initial lithium layer thickness and $l \ll d$. This $D_\perp$ value for lithium diffusion is very large in comparison with the diffusion constant of hydrogen atom in isotropic graphite at room temperature $\sim 5 \times 10^{-17}$ cm^2/s [15]. Only few studies done in the field of lithium-ion batteries have published the diffusion constants of lithium in graphites [9–14]. Most of these data, however, refer to in-plane diffusion constant $D_\parallel$ at *high lithium concentration* (LiC_6; 100% of c_M) and *high temperatures* (~700 K), and they show a considerable scatter in the range of the activation energy $E_a = 0.18$–1.3 eV. Ref. [13] reports for diffusion of Li in HOPG at *low concentrations* ($x \ll 1, Li_xC_6$) and *high temperatures* (1000–1300 K), the value of $D_\parallel = (3 \times 10^3 \text{ cm}^2/\text{s}) \exp(-1.83 \text{ eV}/kT)$ and the ratio $D_\parallel/D_\perp \sim 80$ at $T = 1180$ K. From our work we derive $D_\perp$ at *low temperatures* (300 K) and *low concentration* (0–3% of c_M). Combining the present value of $D_\perp$ at 300 K with the previous value of $D_\perp$ at 1180 K available in the literature [13], we obtain an activation energy $E_a = 0.26$ eV and $D_\perp = (4.5 \times 10^{-6} \text{ cm}^2/\text{s}) \exp(-0.26 \text{ eV}/kT)$.

2.4. Influence of hydrogen retention in graphite

The as-received HOPG specimen was exposed to a hydrogen glow discharge plasma for 60 min until the hydrogen retention seems to have been saturated: such saturation is confirmed by monitoring the hydrogen pressure during the discharge [16]. After then, a ~3-μm thick lithium layer (Li areal density $\sim 1.4 \times 10^{17}$/cm^2) is deposited on the hydrogen-containing HOPG (H areal density $\sim 0.8 \times 10^{17}$/cm^2), and subsequently the specimen is examined by RBS as in the hydrogen-free case. When comparing the data with the hydrogen-free case, the Li-induced hump shrinks more rapidly at the same observation time. Such behavior is markedly seen in Fig. 3, where the lithium amount $N(t)/N_0$ outside the graphite surface is plotted as a function of time. The lithium deposited on the hydrogen-containing graphite disappears at $t = 18$ min while it takes ~36 min in case of the hydrogen-free graphite. Comparison of the experimental points with the theoretical analysis by Eq. (1) suggests a diffusion constant to be $D_\perp = 4.3 \times 10^{-10}$ cm^2/s which is two times larger than that derived for the hydrogen-free HOPG sample.

There are several effects that could explain the observed hydrogen-enhanced Li diffusion. The hydrogen glow discharge at 300 V gives the H retention in the graphite surface layer of ~20 nm in thickness, where $H/C \sim 0.3$. In studies carried out in the field of Li-ion batteries, it was observed that carbon materials containing substantial amount of hydrogen (i.e., $H/C \sim 0.2$) can intercalate more Li atoms in proportion to the H/C atomic ratio [14]. Li atoms are also believed to bind in the vicinity of H atoms, but it is unlikely that bulk lithium hydride (LiH) could be formed in graphites [14]. Another explanation might be that the presence of H induces an increase in spacing between carbon layers [19], which will in turn could facilitate Li diffusion. Finally, the Li diffusion may be accelerated by the formation of surface and near-surface defects in the HOPG sample formed during the 60-min hydrogen glow discharge.

3. Implication of lithium interaction in conditioning effects

In present-day fusion machines, graphite or carbon-based materials often occupy 50–90% of the entire wall area. In such environment, the deposited lithium layer of thickness l will rapidly diffuse into the graphite walls in a time scale of $\tau_L = (2l/\pi)^2/D$. The effective diffusion constant D depends on the temperature and the type of carbon materials and the morphology modified by the hydrogen plasmas. The $D_\perp$ value of HOPG at 300 K obtained in the present study could represent a lower limit, whereas $D_\parallel$ may be two orders of magnitude larger than $D_\perp$. Thus, taking for example $l = 100$ nm at 300 K, $D_\perp = 2 \times 10^{-10}$ cm^2/s and $D_\parallel = 100 D_\perp$. This gives a diffusion time in the range $\tau_L = 10$ ms – 1 s. The Li density near the graphite surface decreases in time from c_0 to c_M, and eventually to c_∞ as the time $t \to \infty$. Typical lithium conditioning effects such as hydrogen gettering and impurity suppression are expected to be proportional to the surface coverage of lithium (Li concentration near surface). Therefore, strong lithium effects are expected only for a short time interval ($\leqslant \tau_L$) between the Li deposition and the plasma discharge. If $t \gg \tau_L$, the lithium effects will be larger for the larger stationary Li density c_∞ (larger Li surface coverage). One could explain the remarkable Li effects in TFTR taking account of the short time interval (~1 s), the large c_∞ (~20 g of Li deposited during five years), and the small value of D due to the low wall temperature (room temperature). In addition, the H retention in graphite was thoroughly reduced in TFTR by helium discharges before Li deposition, thus decreasing the Li diffusion constant.

Lithium insertion into carbonaceous materials is known to occur universally in hundreds of carbon materials [14]. The Li-induced suppression of *physical sputtering* of isotropic graphite [5] cannot be explained without taking into account of lithium–graphite intercalation: TRIM–SP [20] simulation of graphite sputtering shows little change in the carbon sputtering yield with and without 14% Li (c_M). As shown previously [5],

lithium atoms at the graphite surface act as a barrier for carbon sputtering. Once lithium atoms are sputtered away, new Li atoms are promptly supplied to the surface from the graphite bulk owing to the large diffusion constant. On the other hand, the lithium conditioning also suppresses *chemical sputtering* of graphite as reported previously [6]. In this case, the methane formation by hydrogen surface reaction on graphite will be suppressed in proportion to the surface coverage of lithium over carbon layer.

4. Conclusion

Lithium atoms deeply diffuse into the bulk of graphite when metallic lithium is deposited on the graphite surface. This Li–graphite intercalation is essential to explain some of the known lithium conditioning effects observed in tokamaks. Rutherford backscattering spectrometry enabled to measure the perpendicular diffusion constant of lithium in the hydrogen-free HOPG. The result is expressed as $D_\perp = (4.5 \times 10^{-6}\ \mathrm{cm^2/s}) \exp(-0.26\ \mathrm{eV}/kT)$, while the parallel diffusion constant $D_\parallel$ is about two orders of magnitude larger than $D_\perp$. In addition, the presence of hydrogen in the graphite matrix enhances the value of $D_\perp$ by a factor of two. A thin layer (thickness l) of deposited lithium is absorbed by graphite in a diffusion time $\tau_L = (2l/\pi)^2/D$ for the effective diffusion constant D. In order to obtain a marked Li effects, it is recommended that the interval between the lithium deposition and the main discharge is not longer than τ_L. Also, one could make the τ_L value large by reducing the H retention in graphite and by lowering the wall temperature. Further measurements of diffusion constant of lithium in isotropic graphite, carbon–fiber–composite and amorphous carbon are in progress.

References

[1] D. Mansfield et al., Phys. Plasmas 3 (1996) 1.
[2] C.H. Skinner et al., J. Nucl. Mater. 241–243 (1997) 214.
[3] H. Sugai, H. Toyoda, K. Nakamura, K. Furuta, M. Ohori, K. Toi, S. Hirokura, K. Sato, J. Nucl. Mater. 220–222 (1995) 254.
[4] J.T. Hogan, C.E. Bush, C.H. Skinner, Nucl. Fus. 37 (1997) 705.
[5] S. Kato, M. Watanabe, H. Toyoda, H. Sugai, J. Nucl. Mater. 266–269 (1999) 406.
[6] H. Toyoda, M. Watanabe, H. Sugai, J. Nucl. Mater. 241–243 (1997) 1031.
[7] G.L. Jackson, R. Bastasz et al., presented at the Workshop on Lithium Effects in Plasmas, 17–18 October 1996, Princeton.
[8] Y. Hirooka et al., J. Nucl. Mater. 274 (1999) 320.
[9] A. Magerl, H. Zabel, I.S. Anderson, Phys. Rev. Lett. 55 (1985) 222.
[10] P. Freilaender, P. Heitjans, H. Ackermann, B. Bader, G. Kiese, A. Schirmer, H.J. Stoeckmann, C. Van der Marel, Z. Phys. Chem. Neue Falge. 151 (1987) 93.
[11] D.P. Di Vincenzo, E.J. Mele, Phys. Rev. Lett. 53 (1984) 52.
[12] D.A. Morton-Blake, J. Corish, Phys. Rev. B 37 (1988) 4180.
[13] B. Jungblut, E. Hoinkis, Phys. Rev. 40 (1989) 10811.
[14] J.K. Dahn, T. Zheng, Y. Liu, J.S. Xue, Science 270 (1995) 590.
[15] K. Morita, K. Ohtsuka, Y. Hasebe, J. Nucl. Mater. 162–164 (1989) 990.
[16] R.A. Langley, J. Vac. Sci. Technol. A 5 (1987) 2205.
[17] M.F. Smith, J.B. Whitley, D.E. Post, R. Behrrish (Eds.), Physics of Plasma–Wall Interactions in Controlled Fusion, Plenum, New York, 1984, p. 544.
[18] M.D. Mikhailov, M.N. Ozisik, Unified Analysis and Solutions of Heat and Mass Diffusion, Wiley, New York, 1984, p. 287.
[19] Y. Gotoh, H. Shimizu, H. Murakami, J. Nucl. Mater. 162–164 (1989) 851.
[20] J.P. Biersack, W. Eckstein, Appl. Phys. A 34 (1984) 73.